

000  
001  
002054  
055  
056003  
004  
005  
006  
007057  
058  
059  
060  
061008  
009  
010  
011  
012062  
063  
064  
065  
066013  
014  
015067  
068  
069016  
017  
018  
019  
020070  
071  
072  
073  
074021  
022  
023  
024  
025075  
076  
077  
078  
079026  
027  
028  
029  
030080  
081  
082  
083  
084031  
032  
033  
034  
035  
036  
037  
038  
039  
040  
041  
042  
043  
044  
045  
046  
047  
048  
049  
050  
051  
052  
053085  
086  
087  
088  
089  
090  
091  
092  
093  
094  
095  
096  
097  
098  
099  
100  
101  
102  
103  
104  
105  
106  
107

# External Patch Group Prior Guided Internal Subspace Learning for Real Image Denoising

Anonymous CVPR submission

Paper ID \*\*\*\*

## Abstract

Existing image denoising methods largely depends on noise modeling and estimation. The commonly used noise models, additive white Gaussian, are inflexible in describing the complex noise on real noisy images. This would limit the performance of existing methods on denoising real noisy images. In this paper, we firstly demonstrate that almost all state-of-the-art methods on removing Gaussian noise and real noise are limited in denoising real noisy images. We demonstrate that a simple Patch Group based Prior Learning model on RGB images can achieve better performance than existing denoising methods, especially the ones designed for real noise in natural images. Besides, we employ the external patch group prior learning for internal clustering and subspace learning. This external information guided internal denoising methods achieves even better than the external PG prior based methods and the fully internal PG prior based method. Through extensive on standard datasets on real noisy images with groundtruth, we demonstrate that the proposed method achieves much better denoising performance than the other state-of-the-art methods on Gaussian noise removal and real noise removal.

## 1. Introduction

Image denoising is a fundamental problem in computer vision and image processing. It is an ideal platform for testing natural image models and provides high-quality images for other computer vision tasks such as image registration, segmentation, and pattern recognition, etc. For several decades, there emerge numerous image denoising methods [1, 2, 3, 4, 5, 6, 7, 8, 9, 10, 11], and all of them focus mainly on dealing with additive white Gaussian noise (AWGN). However, the images captured by CMOS or CCD cameras will undertake an in-camera imaging pipeline. The in-camera imaging pipeline includes mainly image demosaicing, white balance and color space transform, gamut mapping, tone mapping, and JPEG compression [12, 13].

Therefore, the noise in real images are much more complex than Gaussian, and depends on camera series, brands, as well as the settings (ISO, shutter speed, and aperture, etc). The models designed to deal with AWGN would become much less effective on real noisy images.

In the last decade, the methods of [14, 15, 16, 17, 18, 19, 13] are designed to deal with real noisy images. Almost all these methods coincidentally employ a two-stage framework: in the first stage, assuming a distribution model (usually Gaussian) on the noise and estimate its parameters; in the second stage, performing denoising with the help of the noise modeling and estimation in the first stage. However, the Gaussian assumption is inflexible in describing the complex noise on real noisy images [16]. Although the mixture of Gaussians (MoG) model is possible to approximate any unknown noise [19], estimating its parameters is often time consuming via nonparametric Bayesian techniques [19, 20]. To evaluate the performance of these methods on dealing with complex real noise, we apply these methods, with corresponding default parameters, on a real noisy image provided in [13]. This image is captured by a Nikon D800 camera while the ISO is set as 3200. The "ground truth" image is also provided with which we can calculate objective measurements. More details about this dataset can be found at the experimental section. The denoised images are listed in Figure 1, from which we can see that these methods either remove the noise or oversmooth the complex details in real noisy image. This proves that the above mentioned methods are not effective on denoising complex noise on real images.

In this paper, we attempt to deal with complex noise in real images by integrating the external and internal information. Since the real noise is signal dependent [13, 23], the prior information in external natural images can be employed to avoid the high correlation between noise and signal in internal images. On the other hand, the internal prior is adaptive to the image and can recover better the latent clean image. Based on these observations, we make detailed study on internal and external information for real image denoising task. We made several observa-

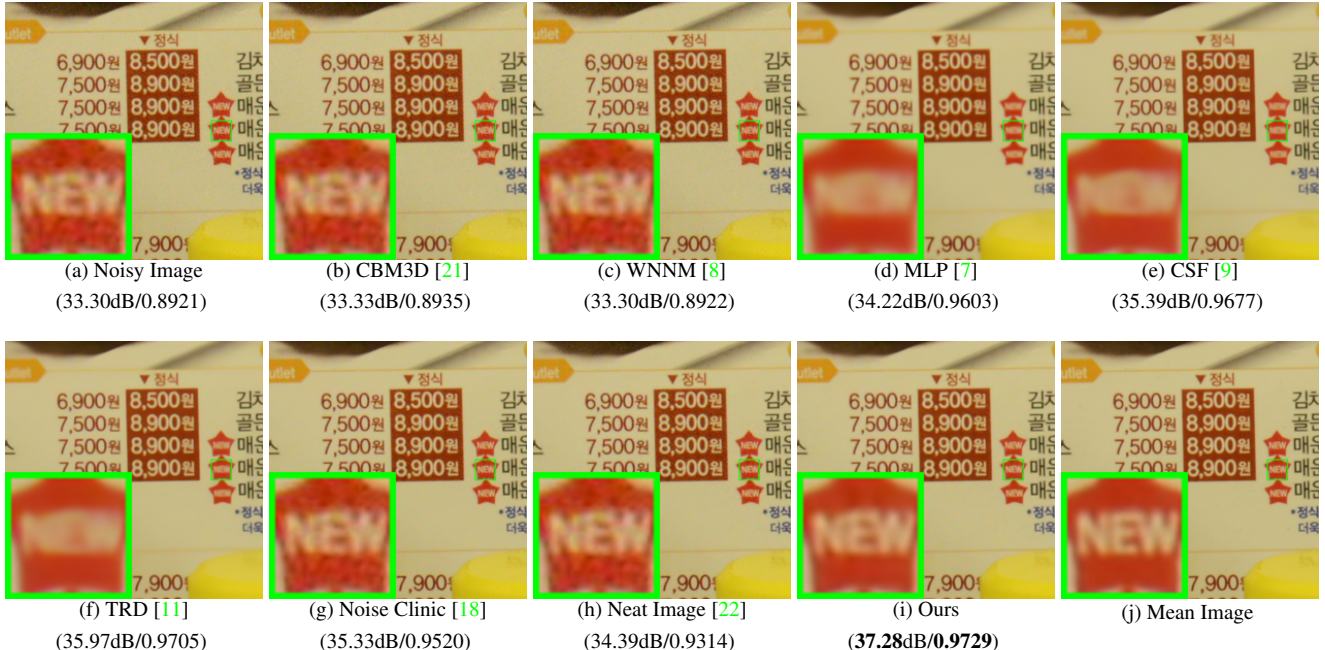


Figure 1. Denoised images of the real noisy image “*Nikon D800 ISO3200 A3*” by different methods. The images are better to be zoomed on screen.

tions. Firstly, we found that the Patch Group Prior learning based denoising method [10] learned on clean RGB images are enough to outperform the above mentioned denoising methods. Secondly, we also found that a fully internal PG prior based denoising method which achieve better performance than the fully external method. Most importantly, we found that the external PG prior guided internal method can achieve even better and faster performance on real image denoising. In fact, the external PG prior learning based model is employed to guide the clustering of internal PGs extracted from the input noisy images. Then for each cluster of PGs, we perform subspace learning by PCA and denoising by weighted sparse coding. We perform comprehensive experiments on real noisy images captured by different CMOS or CCS sensors. The results demonstrate that our method achieves comparable or even better performance on denoising real noisy images. An initial glimpse of our method is also listed in Figure 1. This reveals the potential advantages of combining external and internal information of natural images on robust and complex real noisy image denoising problem.

## 1.1. Our Contributions

The contributions of this paper are summarized as follows:

- We propose a novel method which combine the external and internal PG prior for real noisy image denoising problem;

- Our method doesn’t need noise modeling and estimation, and the noise levels of real noisy images are automatically expressed by the singular values of learned subspace;
- We achieve much better performance on visual quality, PSNR, SSIM, and speed, than other competing methods for real image denoising problem.

The rest of this paper will be summarized as follows: in Section 2, we will introduce the related work close to our work; in Section 3, we will introduce our proposed external prior guided internal subspace learning framework for real image denoising; in Section 4, we will demonstrate the denoising experiments on several standard dataset; in Section 5, we will conclude our paper and give our future work.

## 2. Related Work

### 2.1. Patch Group Prior of Natural Images

The Patch Group (PG) prior [10] is proposed to directly model the non-local self similar (NSS) property of natural images. The NSS property is commonly used in image restoration tasks [1, 4, 5, 8, 10]. The PG prior largely reduces the space of images to be modeled when compared to the patch prior [6]. The better modeling on NSS is demonstrated via better image denoising performance on natural images. However, in [10], only the PGs of clean natural images is utilized, while the PGs of noisy input images are ignored. In this paper, we aim at making use of both PGs

216 from natural clean images and real noisy images for better  
217 denoising performance.  
218

## 219 2.2. Internal v.s. External Image Denoising

220 For natural images, the internal patch recurrence across  
221 multiple scales has been successfully applied in many  
222 image restoration problems [24, 25, 26, 27]. These  
223 work demonstrate that internal information is enough for  
224 many ill-posed problems including denoising additive white  
225 Gaussian noise. The rationale is, since the AWGN noise is  
226 independent of the original clean images, it will be reduced  
227 if the image is scaled to a smaller size. However, the noise  
228 in real images is generated mostly from the camera sensors,  
229 which is highly complex and signal dependent [13]. Be-  
230 sides, according to the seminar workd of [23], the noise in  
231 real images has fixed patterns from several main sources.  
232 Therefore, we can hardly seperate the complex noise from  
233 the signals without the help of external (correct) informa-  
234 tion of natural clean images. Only using the internal infor-  
235 mation may be not enough for real image denoising prob-  
236 lem. On the other hand, the methods only using the ex-  
237 ternal information may be not adaptive for real noisy images.  
238 Recently, the methods of [7, 9, 11] had been proposed to  
239 learn, on both internal and external images, a process di-  
240 rectly mapping the noisy patches to denoised ones. These  
241 discriminative learning based methods are only effective on  
242 additive white Gaussian noise and ineffective on complex  
243 and signal dependent noise in real images. This has been  
244 shown in Figure 1. In this paper, wour goal is to make use  
245 of external information to guide the subspace learning of  
246 internal PGs for image denoising task.  
247

## 248 2.3. Real Image Denoising

249 To the best of our knowledge, the study of real image  
250 denoising can be dated back to the BLS-GSM model [28],  
251 in which Portilla et al. proposed to use scale mixture of  
252 Gaussian in overcomplete oriented pyramids to estimate the  
253 latent clean images. In [14], Portilla proposed to use a cor-  
254 related Gaussian model for noise estimation of each wavelet  
255 subband. Based on the robust statistics theory [?], the work  
256 of Rabie [15] modeled the noisy pixels as outliers, which  
257 could be removed via Lorentzian robust estimator. In [16],  
258 Liu et al. proposed to use ‘noise level function’ (NLF) to es-  
259 timate the noise and then use Gaussian conditional random  
260 field to obtain the latent clean image. Recently, Gong et al.  
261 proposed an optimization based method [17], which mod-  
262 els the data fitting term by weighted sum of  $\ell_1$  and  $\ell_2$  norms  
263 and the regularization term by sparsity prior in the wavelet  
264 transform domain. Later, Lebrun el al. proposed a multi-  
265 scale denoising algorithm called ‘Noise Clinic’ [18] for  
266 real image denoising task. This method generalizes the NL-  
267 Bayes [29] to deal with signal, scale, and frequency depen-  
268 dent noise. Recently, Zhu et al. proposed a Bayesian model  
269

[19] which approximates the noise via Mixture of Gaussian  
270 (MoG) model [20]. The clean image is recovered from the  
271 noisy image by the proposed Low Rank MoG filter (LR-  
272 MoG). However, noise level estimation is already a chal-  
273 lenging problem and denoising methods are quite sensitive  
274 to this parameter. Moreover, these methods are based on  
275 shrinkage models that are too simple to reflect reality, which  
276 results in over-smoothing of important structures such as  
277 small-scale text and textures.  
278

## 279 3. External Patch Group Prior Guided Inter- 280     nal Subspace Learning

281 In this section, we formulate the framework of external  
282 Patch Group prior guided internal subspace learning. We  
283 first introduce the patch group prior leaning on clean natural  
284 RGB images. Then we formulate the external guided inter-  
285     nal subspace learning. Finally, we discuss the differences  
286 between external subspaces and the corresponding internal  
287 subspace.  
288

### 289 3.1. External Patch Group Prior Learning

290 Natural images often demonstrate repetitive patterns,  
291 this nonlocal self-similarity (NSS) property is a key suc-  
292 cessful factor for many image denoising methods [1, 4, 5,  
293 30, 8, 10] and restoration methods [ ]. In [10], the NSS prop-  
294 erty is directly learned as an external prior in a patch group  
295 manner. In this section, we formulate the Patch Group prior  
296 on natural color images.  
297

298 In [10], the patch group (PG) is defined as a group of  
299 similar patches to the local patch. The patch group mean  
300 is destracted, and hence different groups patches can share  
301 similar PGs. Therefore the space to be modeled is largely  
302 reduced. In this work, we extract PGs from RGB im-  
303 ages. Each patch is of size  $p \times p \times 3$ . For each local  
304 patch, we search its similar patches around it through the  
305 Euclidean distance in a local window of size  $W \times W$ .  
306 The PG is denoted by  $\{\mathbf{x}_m\}_{m=1}^M$ , where  $\mathbf{x}_m \in \mathbb{R}^{3p^2 \times 1}$   
307 is a color image patch vector. The mean vector of this  
308 PG is  $\boldsymbol{\mu} = \frac{1}{M} \sum_{m=1}^M \mathbf{x}_m$ , and  $\bar{\mathbf{x}}_m = \mathbf{x}_m - \boldsymbol{\mu}$  is the  
309 group mean subtracted patch vector. The PG is defined as  
310  $\bar{\mathbf{X}} \triangleq \{\bar{\mathbf{x}}_m\}, m = 1, \dots, M$ , and it represent the external  
311 NSS prior on color images. Assume we have extracted  $N$   
312 PGs from a given set of natural images, and the  $n$ -th PG  
313 is defined as  $\bar{\mathbf{X}}_n \triangleq \{\bar{\mathbf{x}}_{n,m}\}_{m=1}^M, n = 1, \dots, N$ . We employ  
314 the patch group based Gaussian Mixture Model (PG-GMM)  
315 for NSS prior learning. We aim to learn a set of  $K$  Gaus-  
316 sians  $\{\mathcal{N}(\boldsymbol{\mu}_k, \Sigma_k)\}$  from  $N$  training PGs  $\{\bar{\mathbf{X}}_n\}$ , while  
317 requiring that all the  $M$  patches  $\{\bar{\mathbf{x}}_{n,m}\}$  in PG  $\bar{\mathbf{X}}_n$  belong to  
318 the same Gaussian component and assume that the patches  
319 in the PG are independently sampled. Note that such an as-  
320 sumption is commonly used in patch based image modeling  
321

324 [3, 5]. Then, the likelihood of  $\{\bar{\mathbf{X}}_n\}$  can be calculated as  
 325

$$P(\bar{\mathbf{X}}_n) = \sum_{k=1}^K \pi_k \prod_{m=1}^M \mathcal{N}(\bar{\mathbf{x}}_{n,m} | \boldsymbol{\mu}_k, \boldsymbol{\Sigma}_k). \quad (1)$$

326 By assuming that all the PGs are independently sampled,  
 327 the overall objective log-likelihood function is  
 328

$$\ln \mathcal{L} = \sum_{n=1}^N \ln \left( \sum_{k=1}^K \pi_k \prod_{m=1}^M \mathcal{N}(\bar{\mathbf{x}}_{n,m} | \boldsymbol{\mu}_k, \boldsymbol{\Sigma}_k) \right). \quad (2)$$

329 We maximize the above objective function for PG-GMM  
 330 learning. Finally, we obtain the GMM model with three sets  
 331 of parameters including mixture weights  $\{\pi_k\}_{k=1}^K$ , mean  
 332 vectors  $\{\boldsymbol{\mu}_k = \mathbf{0}\}_{k=1}^K$ , and covariance matrices  $\{\boldsymbol{\Sigma}_k\}_{k=1}^K$ .  
 333 Noted that in PGPD [10], the mean vector of each cluster is  
 334 natural zeros, i.e.,  $\boldsymbol{\mu}_k = \mathbf{0}$ .  
 335

### 3.2. External PG Prior Guided Internal Subspace Learning

341 For each  $\bar{\mathbf{Y}}$ , we select the most suitable Gaussian component  
 342 to it from the trained PG-GMM. Since the noise on  
 343 real images are small when compared to the signals and the  
 344 noise on real images are dependent on the signals, the covari-  
 345 ariance matrix of the  $k$ th component is still  $\boldsymbol{\Sigma}_k$ . The selec-  
 346 tion can be done by checking the posterior probability that  
 347  $\bar{\mathbf{Y}}$  belongs to the  $k$ th Gaussian component:  
 348

$$P(k|\bar{\mathbf{Y}}) = \frac{\prod_{m=1}^M \mathcal{N}(\bar{\mathbf{y}}_m | \mathbf{0}, \boldsymbol{\Sigma}_k)}{\sum_{l=1}^K \prod_{m=1}^M \mathcal{N}(\bar{\mathbf{y}}_m | \mathbf{0}, \boldsymbol{\Sigma}_l)}. \quad (3)$$

351 Finally, the component with the highest probability  
 352  $\ln P(k|\bar{\mathbf{Y}})$  is selected to process  $\bar{\mathbf{Y}}$ .  
 353

354 Suppose that the  $k$ th Gaussian component is selected for  
 355 PG  $\bar{\mathbf{Y}}$ . For notation simplicity, we remove the subscript  
 356  $k$  and denote by  $\boldsymbol{\Sigma}$  the covariance matrix of this compo-  
 357 nent. In PG-GMM, the PGs actually represent the varia-  
 358 tions of the similar patches in a group, and these varia-  
 359 tions are assigned to the same Gaussian distribution. By  
 360 singular value decomposition (SVD),  $\boldsymbol{\Sigma}$  can be factorized  
 361 as  $\boldsymbol{\Sigma} = \mathbf{D}\boldsymbol{\Lambda}\mathbf{D}^T$ , where  $\mathbf{D}$  is an orthonormal matrix com-  
 362 posed by the eigenvectors of  $\boldsymbol{\Sigma}$  and  $\boldsymbol{\Lambda}$  is the diagonal matrix  
 363 of eigenvalues. With PG-GMM, the eigenvectors in  $\mathbf{D}$  cap-  
 364 ture the statistical structures of NSS variations in natural  
 365 images, while the eigenvalues in  $\boldsymbol{\Lambda}$  represent the significance  
 366 of these eigenvectors. Fig. 4 shows the eigenvectors for 3  
 367 Gaussian components. It can be seen that these eigenvectors  
 368 encode the possible variations of the PGs. For one Gaussian  
 369 component, the first eigenvector represents its largest varia-  
 370 tion, while the last eigenvector represents its smallest varia-  
 371 tion. For different Gaussian components, we can see that  
 372 their eigenvectors (with the same index) are very different.  
 373 Hence,  $\mathbf{D}$  can be used to represent the structural variations  
 374 of the PGs in that component.  
 375

$$\min_{\boldsymbol{\alpha}} \|\bar{\mathbf{y}}_m - \mathbf{D}\boldsymbol{\alpha}\|_2^2 + \sum_{i=1}^{p^2} \frac{c}{\lambda_i} |\alpha_i|. \quad (4)$$

376 By comparing (??) with (??), we can see that the  $i$ th entry  
 377 of the weighting vector  $\mathbf{w}$  should be  
 378

$$\mathbf{w}_i = c/(\lambda_i + \varepsilon), \quad (5)$$

379 where  $\varepsilon$  is a small positive number to avoid dividing by zero.  
 380 With  $\mathbf{w}$  determined by (??), let's see what the solution of  
 381 (??) should be. Since the dictionary  $\mathbf{D}$  is orthonormal, it  
 382 is not difficult to find out that (??) has a closed-form solu-  
 383 tion (detailed derivation can be found in the supplementary  
 384 material):  
 385

$$\hat{\boldsymbol{\alpha}} = \text{sgn}(\mathbf{D}^T \bar{\mathbf{y}}_m) \odot \max(|\mathbf{D}^T \bar{\mathbf{y}}_m| - \mathbf{w}/2, 0), \quad (6)$$

386 where  $\text{sgn}(\bullet)$  is the sign function,  $\odot$  means element-wise  
 387 multiplication, and  $|\mathbf{D}^T \bar{\mathbf{y}}_m|$  is the absolute value of each  
 388 entry of vector  $|\mathbf{D}^T \bar{\mathbf{y}}_m|$ . The closed-form solution makes  
 389 our weighted sparse coding process very efficient.  
 390

### 3.3. What does External Data help the Internal Subspace Learning?

391 The external data can help the internal learning in two  
 392 ways. On one hand, it can guide the noisy image patches to  
 393 be divided into correct subspaces through clustering. If we  
 394 cluster the noisy patches in an automatical way, just like the  
 395 PLE [31] did, the signal dependent noise would be hardly  
 396 removed. With the help of clean external data, the noisy  
 397 patches can be divided into correct subspaces. Besides, ex-  
 398 ternal data guided internal clustering is much more efficient  
 399 than directly clustering the noisy data due to the time con-  
 400 suming fitting procedure. On the other hand, due to the  
 401 correct division of internal noisy data, the dictionary and  
 402 pariters for subspace learning could be more adaptive to  
 403 the testing real noisy image. Hence, it would achieve bet-  
 404 ter denoising performance than the methods only using the  
 405 external information.  
 406

### 3.4. The Internal PGs Spaces Are Subspaces of Corresponding External PG Spaces

417 In this subsection, we compare the distribution of exter-  
 418 nal PGs extracted from clean natural images and real noisy  
 419 images. For better illumination, we randomly selected a  
 420 cluster and project the original clean PGs onto a 2-D plane.  
 421 Plot a Figure to demonstrate the data distributed in external  
 422 space and the assigned internal subspace. The internal sub-  
 423 space is only a subspace of the external space. Hence, if we  
 424 use the external data to perform denoising, the performance  
 425 would be limited due to the dependence of noise on signal.  
 426 If we combine the external and internal data for subspace  
 427 learning, the learned subspace would be too generative and  
 428 would therefore not specifically suitable for the testing data.  
 429

## 432 4. The Enhanced Algorithm 486

### 433 4.1. Iterative Regularization 487

436 Perform image denoising in one iteration is not  
 enough for real noise since the noise is signal dependent.  
 The removed noise in one iteration is largely dependent on  
 the signal. Therefore, it is essential to add back some residuals  
 removed in this iteration for the denoising of the next  
 iteration.

### 442 4.2. Effectively dealing with different noisy images 490

444 For real image denoising, we can perform well on images  
 which have similar noise levels with the training dataset.  
 How can we deal with the real noisy images whose noise  
 levels are higher than the training dataset? The answer is  
 to remove the noise by more iterations. The input image of  
 each iteration is the recovered image of previous iteration.  
 This makes sense since we can still view the recovered image  
 as a real noisy image.

452 This will also bring a second problem, that how we could  
 automatically terminate the iteration. This can be solved  
 by two methods. One way is to compare the images between  
 two iterations and calculate their difference, the iteration  
 can be terminated if the difference is smaller than a threshold.  
 The other way is to estimate the noise level of the current image  
 and terminate the iterations when the noise level is lower than a preset threshold. We employ the  
 second way and set the threshold as 0.0001 in our experiments.  
 In fact, most of our testing images will be denoised  
 well in one iteration.

### 464 4.3. Efficient Model Selection by Gating Network 500

466 In the Gaussian component selection procedure, if we  
 employ the full posterior estimation, the speed is not fast.  
 Our algorithm can be speeded up by introducing the Gating  
 network model.

### 470 4.4. The Overall Algorithm 504

472 With the solution  $\hat{\alpha}$  in (??), the clean patch in a PG can  
 be estimated as  $\hat{x}_m = \mathbf{D}\hat{\alpha} + \mu_y$ . Then the clean image  $\hat{x}$   
 can be reconstructed by aggregating all the estimated PGs.  
 In practice, we could perform the above denoising procedures  
 for several iterations for better denoising outputs. In  
 iteration  $t$ , we use the iterative regularization strategy [?]  
 to add back to the recovered image  $\hat{x}^{(t-1)}$  some estimation  
 residual in iteration  $t-1$ . The standard deviation of noise in  
 iteration  $t$  is adjusted as  $\sigma^{(t)} = \eta * \sqrt{\sigma^2 - \|\mathbf{y} - \mathbf{y}^{(t-1)}\|_2^2}$ ,  
 where  $\eta$  is a constant. The proposed denoising algorithm is  
 summarized in Algorithm 1 (Alg. 1).

483 In the proposed algorithm, there are  $N$  PGs in an im-  
 age and  $M$  patches in each PG. Then the computational  
 cost for Gaussian component selection is  $O(p^6NMK)$ . The

---

### 482 Alg. 1: Patch Group Prior based Denoising (PGPD) 486

483 **Input:** Noisy image  $\mathbf{y}$ , PG-GMM model 487

484 1. Initialization:  $\hat{\mathbf{x}}^{(0)} = \mathbf{y}, \mathbf{y}^{(0)} = \mathbf{y}$ ; 488

485 **for**  $t = 1 : IteNum$  **do** 489

486   2. Iterative Regularization: 490

$$487 \quad \mathbf{y}^{(t)} = \hat{\mathbf{x}}^{(t-1)} + \delta(\mathbf{y} - \mathbf{y}^{(t-1)}); 491$$

488   3. Estimate the standard deviation of noise; 492

489     **for** each PG  $Y$  **do** 493

490       4. Calculate group mean  $\mu_y$  and form PG  $\bar{Y}$ ; 494

491       5. Gaussian component selection via (??); 495

492       6. Denoising by Weighted Sparse Coding (??); 496

493       7. Recover each patch in this PG via  $\hat{\mathbf{x}}_m = \mathbf{D}\hat{\alpha} + \mu_y$ ; 497

494     **end for** 498

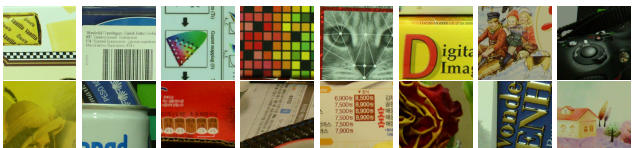
495     8. Aggregate the recovered PGs to form the recovered 499  
 496 image  $\hat{\mathbf{x}}^{(t)}$ ;  
**end for** 500

501 **Output:** The recovered image  $\hat{\mathbf{x}}^{(IteNum)}$ . 502

---



503 Figure 2. Some testing images in the dataset [13]. 504



505 Figure 3. Some cropped images of the dataset [13]. 506

507 cost for iterative regularization and noise estimation is neg-  
 508 ligible. The cost for closed-form weighted sparse coding is  
 509  $O(p^4NM)$ . Suppose that there are  $T$  iterations, the overall  
 510 complexity of our denoising algorithm is  $O(p^6NMKT)$ .  
 511

## 524 5. Experiments 530

525 In this section, we perform real image denoising exper-  
 526 iments on three standard datasets. The first dataset is real  
 527 noisy images with mean images as ground truths provided  
 528 by [13], some samples are shown in Figure 3. The sec-  
 529 ond dataset is provided by the website of Noise Clinic [18].  
 530 The third dataset is provided by the Commercial software  
 531 Neat Image [22]. The second and third dataset do not have  
 532 ground truth images.

540

## 5.1. Parameters Setting

The proposed method contains the PG prior learning stage, the external prior guided internal subspace learning stage, and the denoising stage. In the learning stage, similar to the PGPD, there are four parameters,  $p$ ,  $M$ ,  $W$ , and  $K$ . We set  $p = 6$  and hence the patch size is  $6 \times 6 \times 3$ . The window size for searching PGs is  $W = 31$ . The number of similar patches is  $N = 10$ , the number of clusters is set as  $K = 33$ . In the external prior guided learning stage, there is no parameters. In the denoising stage, there are one parameter, i.e., the  $\lambda$  which is used to regularize the sparse term.

553

## 5.2. Comparison on External and Internal methods

In this subsection, we compared the proposed external prior guided internal subspace learning model on real image denoising. The three methods are evaluated on the dataset provided in [13]. We calculate the PSNR, SSIM [?] and visual quality of these three methods. We also compare the speed. The PSNR and SSIM results on 60 cropped images from [13] are listed in Table 1. The images are cropped into size of  $500 \times 500$  for better illustration. We also compare the three methods on visual quality in Figure 5.2 and Figure 5.2, we can see that the Offline method is better at edges, smooth regions while the Online method is good at complex textures. The reason is two folds. Firstly, the Offline method is learned on clean images and hence is better at representing edges, structures, and smooth area. The online method is influenced by the noise and hence some noise cannot be removed. Secondly, the Online method is better at recovering complex area since they could learn adaptive dictionaries for the specific area. The Offline method cannot recover the complex area since they did not learn the similar structures from the external natural clean images.

577

## 5.3. Comparison With other Competing Methods

We compare with previous state-of-the-art Gaussian noise removal methods such as BM3D [4], WNNM [8], MLP [7], CSF [9], and the recently proposed TRD [11]. We also compare with three competing real image denoising methods such as Noise Clinic, Neat Image, and the CCNoise method proposed recently. The popular software NeatImage which is one of the best denoising software available. All these methods need noise estimation which is very hard to perform if there is no uniform regions available in the testing image. The NeatImage will fail to perform automatical parameters settings if there is no uniform regions.<sup>1</sup>

591

<sup>1</sup>To compare with CCNoise, we first transform the denoised images into double format.

592

593

We the competing denoising methods from various research directions on two datasets. Both the two datasets comes from the [13]. The first dataset contains 17 images of size over  $7000 \times 5000$ . Since this dataset contains recurrent contents across different images, we crop 60 small images of size  $500 \times 500$  from these 17 images in [13].

The PSNR and SSIM results are listed in table 2.

## 5.4. Discussion on Parameter $\lambda$

The proposed method only has a key parameter, namely the regularization parameter  $\lambda$ . To demonstrate that the proposed method is robust to the variance of  $\lambda$ , we vary the parameter  $\lambda$  across a wide range and obtain the PSNR and SSIM results as a function of the parameter  $\lambda$ . The results is shown in Figure 8, from which we can see that the proposed method can achieve a PSNR (SSIM) over 38.2dB (0.9620) when  $\lambda$  varies from  $1e-3$  to  $4e-4$ . This shows that the proposed method is indeed robust to the chosen of the parameter  $\lambda$ .

## 6. Conclusion and Future Work

In the future, we will evaluate the proposed method on other computer vision tasks such as single image super-resolution, photo-sketch synthesis, and cross-domain image recognition. Our proposed method can be improved if we use better training images, fine tune the parameters via cross-validation. We believe that our framework can be useful not just for real image denoising, but for image super-resolution, image cross-style synthesis, and recognition tasks. This will be our line of future work.

## References

- [1] A. Buades, B. Coll, and J. M. Morel. A non-local algorithm for image denoising. *CVPR*, pages 60–65, 2005. [1](#), [2](#), [3](#)
- [2] S. Roth and M. J. Black. Fields of Experts. *International Journal of Computer Vision*, 82(2):205–229, 2009. [1](#)
- [3] M. Elad and M. Aharon. Image denoising via sparse and redundant representations over learned dictionaries. *Image Processing, IEEE Transactions on*, 15(12):3736–3745, 2006. [1](#), [4](#)
- [4] K. Dabov, A. Foi, V. Katkovnik, and K. Egiazarian. Image denoising by sparse 3-D transform-domain collaborative filtering. *Image Processing, IEEE Transactions on*, 16(8):2080–2095, 2007. [1](#), [2](#), [3](#), [6](#)
- [5] J. Mairal, F. Bach, J. Ponce, G. Sapiro, and A. Zisserman. Non-local sparse models for image restoration. *ICCV*, pages 2272–2279, 2009. [1](#), [2](#), [3](#), [4](#)
- [6] D. Zoran and Y. Weiss. From learning models of natural image patches to whole image restoration. *ICCV*, pages 479–486, 2011. [1](#), [2](#)
- [7] Harold C Burger, Christian J Schuler, and Stefan Harmeling. Image denoising: Can plain neural networks compete with

648  
649  
650  
651  
652  
653  
654  
655  
656  
657  
658  
659  
660



Figure 4. Denoised images of the image "Nikon D600 ISO 3200 C1" by different methods. The images are better to be zoomed in on screen.

661  
662  
663  
664  
665  
666  
667  
668  
669  
670  
671  
672

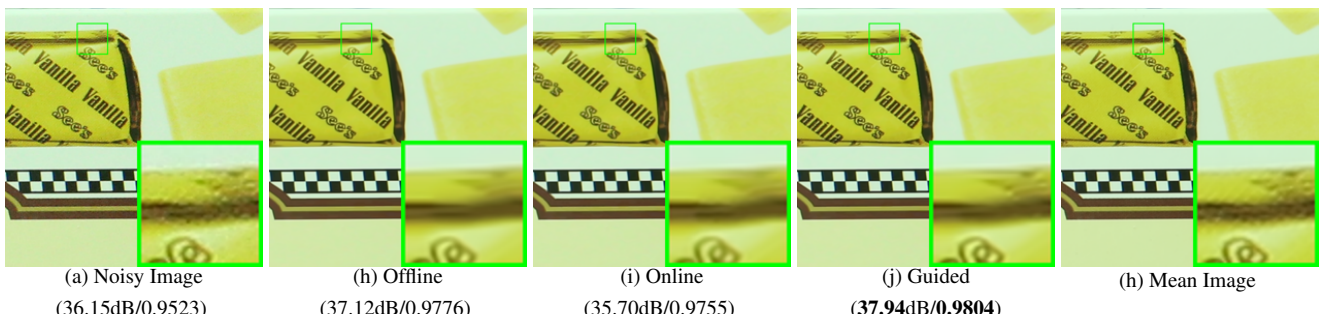


Figure 5. Denoised images of the image "Canon EOS 5D Mark3 ISO 3200 C1" by different methods. The images are better to be zoomed in on screen.

673  
674  
675  
676  
677  
678  
679  
680  
681  
682  
683  
684  
685  
686  
687  
688  
689  
690  
691  
692  
693  
694  
695  
696  
697  
698  
699  
700  
701

bm3d? Computer Vision and Pattern Recognition (CVPR), 2012 IEEE Conference on, pages 2392–2399, 2012. [1](#), [2](#), [3](#), [6](#)

- [8] S. Gu, L. Zhang, W. Zuo, and X. Feng. Weighted nuclear norm minimization with application to image denoising. *CVPR*, pages 2862–2869, 2014. [1](#), [2](#), [3](#), [6](#)
- [9] U. Schmidt and S. Roth. Shrinkage fields for effective image restoration. *Computer Vision and Pattern Recognition (CVPR), 2014 IEEE Conference on*, pages 2774–2781, June 2014. [1](#), [2](#), [3](#), [6](#)
- [10] J. Xu, L. Zhang, W. Zuo, D. Zhang, and X. Feng. Patch group based nonlocal self-similarity prior learning for image denoising. *2015 IEEE International Conference on Computer Vision (ICCV)*, pages 244–252, 2015. [1](#), [2](#), [3](#), [4](#)
- [11] Yunjin Chen, Wei Yu, and Thomas Pock. On learning optimized reaction diffusion processes for effective image restoration. *Proceedings of the IEEE Conference on Computer Vision and Pattern Recognition*, pages 5261–5269, 2015. [1](#), [2](#), [3](#), [6](#)
- [12] S. J. Kim, H. T. Lin, Z. Lu, S. Ssstrunk, S. Lin, and M. S. Brown. A new in-camera imaging model for color computer vision and its application. *IEEE Transactions on Pattern Analysis and Machine Intelligence*, 34(12):2289–2302, Dec 2012. [1](#)
- [13] Seonghyeon Nam, Youngbae Hwang, Yasuyuki Matsushita, and Seon Joo Kim. A holistic approach to cross-channel image noise modeling and its application to image denoising.

702  
703  
704  
705  
706  
707  
708  
709  
710  
711  
712  
713  
714  
715  
716  
717  
718  
719  
720  
721  
722  
723  
724  
725  
726  
727  
728  
729  
730  
731  
732  
733  
734  
735  
736  
737  
738  
739  
740  
741  
742  
743  
744  
745  
746  
747  
748  
749  
750  
751  
752  
753  
754  
755

*Proc. Computer Vision and Pattern Recognition (CVPR)*, pages 1683–1691, 2016. [1](#), [3](#), [5](#), [6](#), [8](#)

- [14] J. Portilla. Full blind denoising through noise covariance estimation using gaussian scale mixtures in the wavelet domain. *Image Processing, 2004. ICIP '04. 2004 International Conference on*, 2:1217–1220, 2004. [1](#), [3](#)
- [15] Tamer Rabie. Robust estimation approach for blind denoising. *Image Processing, IEEE Transactions on*, 14(11):1755–1765, 2005. [1](#), [3](#)
- [16] C. Liu, R. Szeliski, S. Bing Kang, C. L. Zitnick, and W. T. Freeman. Automatic estimation and removal of noise from a single image. *IEEE Transactions on Pattern Analysis and Machine Intelligence*, 30(2):299–314, 2008. [1](#), [3](#)
- [17] Zheng Gong, Zuowei Shen, and Kim-Chuan Toh. Image restoration with mixed or unknown noises. *Multiscale Modeling & Simulation*, 12(2):458–487, 2014. [1](#), [3](#)
- [18] M. Lebrun, M. Colom, and J.-M. Morel. Multiscale image blind denoising. *Image Processing, IEEE Transactions on*, 24(10):3149–3161, 2015. [1](#), [2](#), [3](#), [5](#)
- [19] Fengyuan Zhu, Guangyong Chen, and Pheng-Ann Heng. From noise modeling to blind image denoising. *The IEEE Conference on Computer Vision and Pattern Recognition (CVPR)*, June 2016. [1](#), [3](#)
- [20] C. M. Bishop. *Pattern recognition and machine learning*. New York: Springer, 2006. [1](#), [3](#)
- [21] K. Dabov, A. Foi, V. Katkovnik, and K. Egiazarian. Color image denoising via sparse 3d collaborative filtering with

756 Table 1. Average PSNR(dB) results of different methods on 60 cropped real noisy images captured in [13].  
757

	Noisy	CBM3D	WNNM	MLP	CSF	TRD	NI	NC	Offline	Online	Guided
PSNR	34.51	34.58	34.52	36.19	37.40	37.75	36.53	37.57	38.19	38.07	<b>38.51</b>
SSIM	0.8718	0.8748	0.8743	0.9470	0.9598	0.9617	0.9241	0.9514	0.9663	0.9625	<b>0.9674</b>

761 Table 2. Average PSNR(dB) results of different methods on 15 cropped real noisy images used in [13].  
762

Camera Settings	Noisy	CBM3D	WNNM	MLP	CSF	TRD	NI	NC	CC	Guided
Canon 5D Mark III ISO = 3200	37.00	37.08	37.09	33.92	35.68	36.20	37.68	38.76	38.37	<b>40.32</b>
	33.88	33.94	33.93	33.24	34.03	34.35	34.87	35.69	35.37	<b>37.12</b>
	33.83	33.88	33.90	32.37	32.63	33.10	34.77	35.54	34.91	<b>37.09</b>
Nikon D600 ISO = 3200	33.28	33.33	33.34	31.93	31.78	32.28	34.12	<b>35.57</b>	34.98	35.23
	33.77	33.85	33.79	34.15	35.16	35.34	35.36	<b>36.70</b>	35.95	36.57
	34.93	35.02	34.95	37.89	39.98	40.51	38.68	39.28	<b>41.15</b>	38.73
Nikon D800 ISO = 1600	35.47	35.54	35.57	33.77	34.84	35.09	37.34	38.01	37.99	<b>38.52</b>
	35.71	35.79	35.77	35.89	38.42	38.65	38.57	39.05	<b>40.36</b>	<b>40.36</b>
	34.81	34.92	34.95	34.25	35.79	35.85	37.87	38.20	38.30	<b>38.81</b>
Nikon D800 ISO = 3200	33.26	33.34	33.31	37.42	38.36	38.56	36.95	38.07	<b>39.01</b>	38.32
	32.89	32.95	32.96	34.88	35.53	35.76	35.09	35.72	<b>36.75</b>	<b>36.73</b>
	32.91	32.98	32.96	38.54	40.05	<b>40.59</b>	36.91	36.76	39.06	38.29
Nikon D800 ISO = 6400	29.63	29.66	29.71	33.59	34.08	34.25	31.28	33.49	<b>34.61</b>	33.37
	29.97	30.01	29.98	31.55	32.13	32.38	31.38	32.79	<b>33.21</b>	<b>33.23</b>
	29.87	29.90	29.95	31.42	31.52	31.76	31.40	32.86	33.22	<b>33.29</b>
Average PSNR	33.41	33.48	33.48	34.32	35.33	35.65	35.49	36.43	36.88	<b>37.07</b>
Average SSIM	0.8483	0.8511	0.8512	0.9113	0.9250	0.9280	0.9126	0.9364	0.9481	<b>0.9501</b>

783 grouping constraint in luminance-chrominance space. *IEEE International Conference on Image Processing*, 1, 2007. 2784 [22] Neatlab ABSoft. Neat image. <https://ni.neatvideo.com/home>. 2, 5785 [23] Glenn E Healey and Raghava Kondepudy. Radiometric ccd camera calibration and noise estimation. *IEEE Transactions on Pattern Analysis and Machine Intelligence*, 16(3):267–276, 1994. 1, 3786 [24] Daniel Glasner, Shai Bagon, and Michal Irani. Super-resolution from a single image. *ICCV*, 2009. 3787 [25] Maria Zontak, Inbar Mosseri, and Michal Irani. Separating signal from noise using patch recurrence across scales. *Proceedings of the IEEE Conference on Computer Vision and Pattern Recognition*, pages 1195–1202, 2013. 3788 [26] Tomer Michaeli and Michal Irani. Blind deblurring using internal patch recurrence. *European Conference on Computer Vision*, pages 783–798, 2014. 3789 [27] Y. Bahat and M. Irani. Blind dehazing using internal patch recurrence. *IEEE International Conference on Computational Photography (ICCP)*, pages 1–9, May 2016. 3790 [28] J. Portilla, V. Strela, M.J. Wainwright, and E.P. Simoncelli. Image denoising using scale mixtures of Gaussians in the wavelet domain. *Image Processing, IEEE Transactions on*, 12(11):1338–1351, 2003. 3791 [29] M. Lebrun, A. Buades, and J. M. Morel. A nonlocal bayesian image denoising algorithm. *SIAM Journal on Imaging Sciences*, 6(3):1665–1688, 2013. 3792 [30] W. Dong, L. Zhang, G. Shi, and X. Li. Nonlocally centralized sparse representation for image restoration. *Image Processing, IEEE Transactions on*, 22(4):1620–1630, 2013. 3793 [31] G. Yu, G. Sapiro, and S. Mallat. Solving inverse problems with piecewise linear estimators: From Gaussian mixture models to structured sparsity. *Image Processing, IEEE Transactions on*, 21(5):2481–2499, 2012. 4

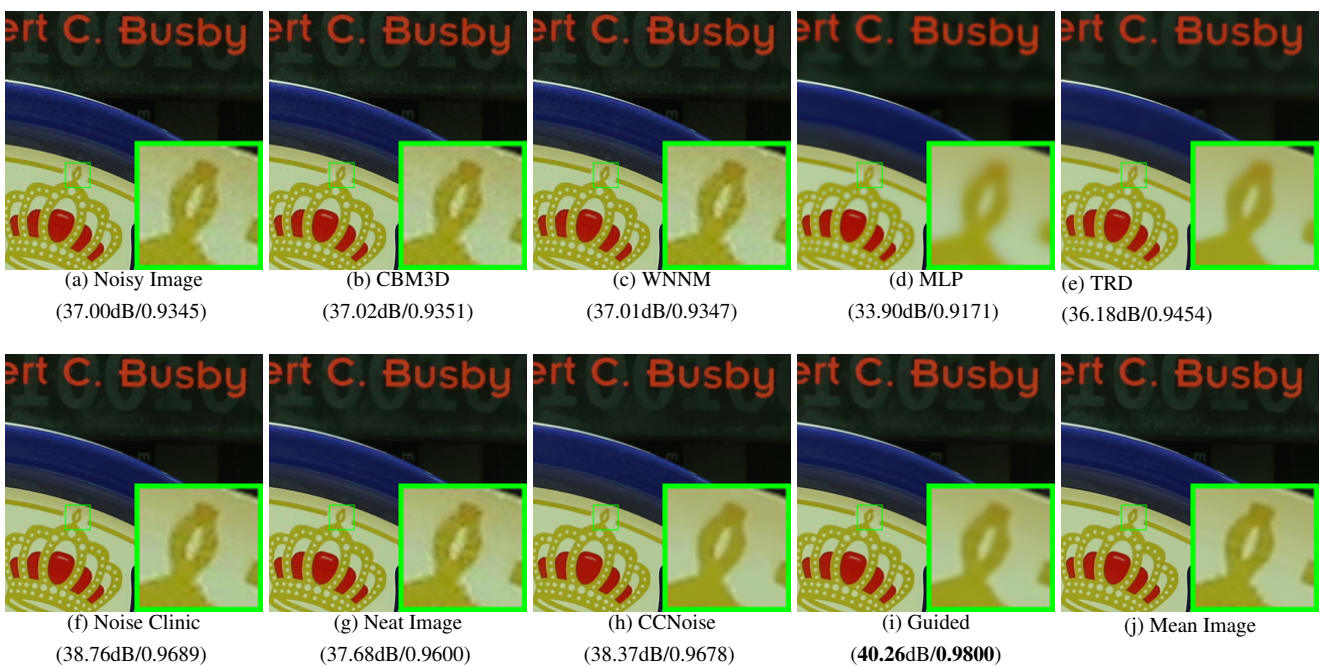


Figure 6. Denoised images of the image "Canon 5D Mark 3 ISO 3200 1" by different methods. The images are better to be zoomed in on screen.

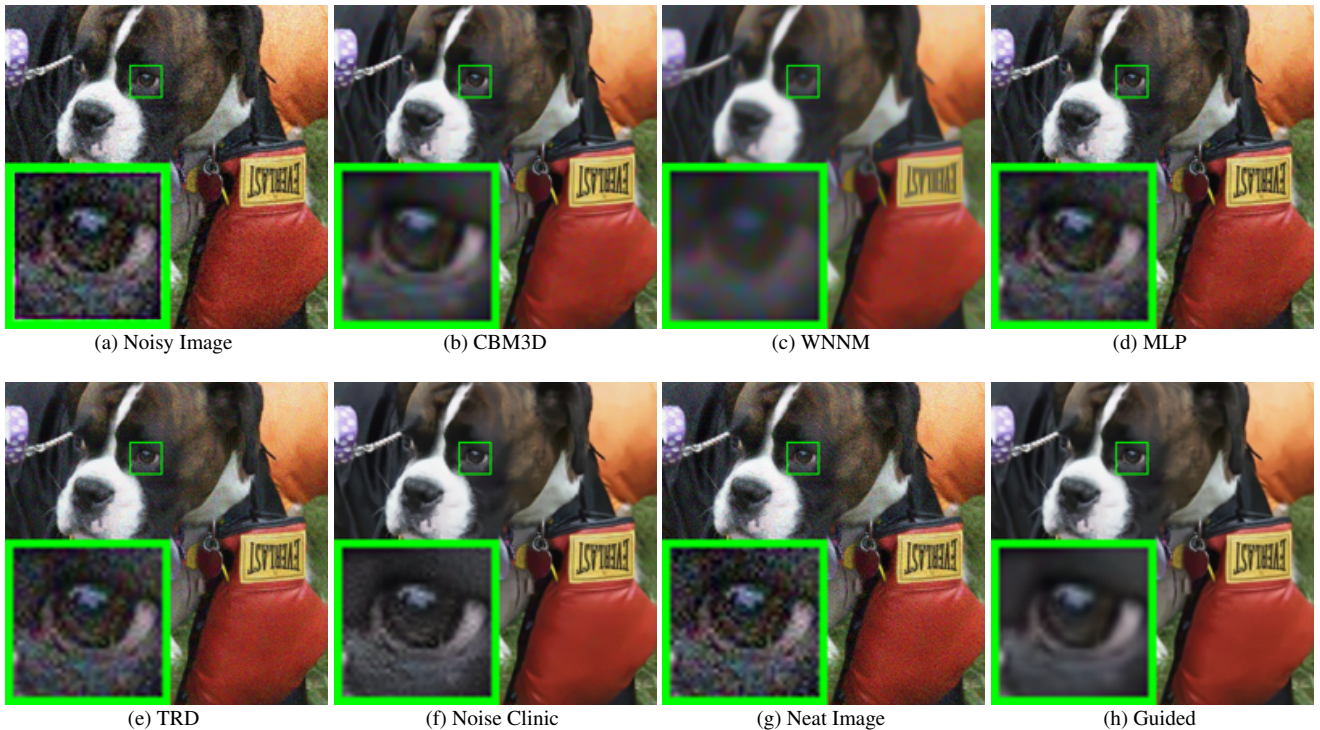


Figure 7. Denoised images of the image "5dmark3iso32003" by different methods. The images are better to be zoomed in on screen.

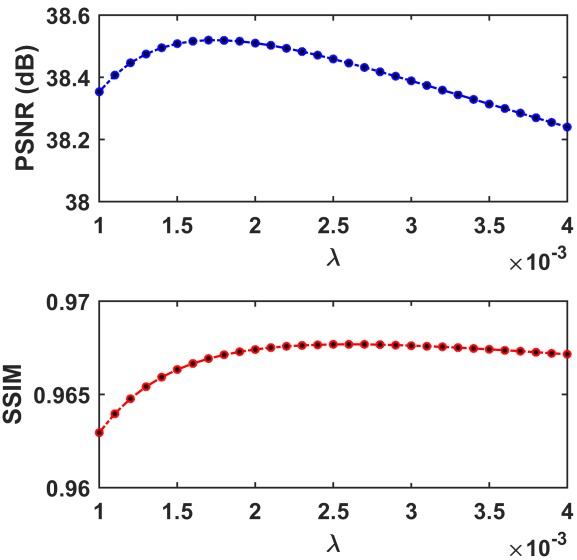


Figure 8. The PSNR/SSIM results as a function of the parameter  $\lambda$ .